Mechanics of Materials 72 (2014) 46–60

Contents lists available at ScienceDirect

Mechanics of Materials

journal homepage: www.elsevier.com/locate/mechmat

Post microbuckling mechanics of fibre-reinforced shape-memory polymers undergoing flexure deformation

Xin Lan [a,b], Liwu Liu [c], Yanju Liu [c], Jinsong Leng [a,*], Shanyi Du [a]

[a] Centre for Composite Materials, Science Park of Harbin Institute of Technology (HIT), P.O. Box 3011, No. 2, YiKuang Street, Harbin 150080, PR China
[b] Dongfang Electric Corporation R&D Centre, No. 18, XiXin Street, Chengdu 611731, PR China
[c] Department of Astronautical Science and Mechanics, Harbin Institute of Technology (HIT), P.O. Box 301, No. 92, West Dazhi Street, Harbin 150001, PR China

ARTICLE INFO

Article history:
Received 1 December 2012
Received in revised form 28 April 2013
Available online 14 June 2013

Keywords:
Shape-memory polymer
Post microbuckling
Fibre

ABSTRACT

The buckling mechanics of fibre-reinforced shape-memory polymer composites (SMPCs) under finite flexure deformation is investigated. The analytical expressions of the key parameters during the buckling deformation of the materials were determined, and the local post-buckling mechanics of the unidirectional fibre-reinforced SMPC were further discussed. The cross section of SMPC under flexural deformation can be divided into three areas: the non-buckling stretching area, non-buckling compression area and buckling compression area. These areas were described by three variables: the critical buckling position, the neutral plane position and the fibre buckling half-wavelength. A strain energy expression of the SMPC thermodynamic system is developed. According to the principle of minimum energy, the analytical expressions of key parameters in the flexural deformation process is determined, including the critical buckling curvature, critical buckling position, position of the neutral plane, wavelength of the buckling fibre, amplitude of the buckling fibre and macroscopic structural strain of the composite material. The results showed that fibre buckling occurred in the material when the curvature increasing from infinitesimal to the critical value. If the curvature is greater than the critical curvature, the neutral plane of the material will move towards the outboard tensile area, and the critical buckling position will move towards the neutral plane. Consequently, the half-wavelength of the buckling fibre was relatively stabilised, with the amplitude increasing dramatically. Along with the increasing of the shear modulus, the critical curvature and buckling amplitude increase, while the critical half-wavelength of the fibre buckling decrease and the critical strain of the composite material increase. Finally, we conducted experiments to verify the correction of the key parameters describing SMPC materials under flexural deformation. The values determined by the experiments proved that the theoretical prediction is correct. Additionally, the buckling deformation of the carbon fibre generated a large macroscopic structural strain of the composite material and obtained a resulting large flexural curvature of the structure with minimal material strain of the carbon fibre.

1. Introductions

It is widely accepted that a film bonded to a compliant substrate often forms a pattern of wrinkles when subjected to a compressive membrane force (Huang et al., 2004, 2005). However, nanowires or nanotubes on the surface of a compliant substrate can also undergo in-surface buckling under mechanical loading conditions (Ryu et al., 2009; Xiao et al., 2010). In the case of nanofibres buried in the interior of compliant substrates, this paper provides

* Corresponding author. Tel./fax: +86 451 86402328.
E-mail address: lengjs@hit.edu.cn (J. Leng).

http://dx.doi.org/10.1016/j.mechmat.2013.05.012
0167-6636/

experimental and theoretical evidence to the buckling of the carbon fibres in response to external loads.

Common compliant substrate materials include electroactive polymers (EAPs) and shape-memory polymers (SMPs). Electroactive polymers can change their shapes or volumes when exposed to external electrical fields, and they can recover their original shapes or volumes once the electrical fields remove. Because of this characteristic, they can be used as smart transducers in application such as novel actuators, sensors and electric generators (Liu et al., 2008, 2009, 2010, 2011; Li et al., 2011; Suo et al., 2008; Suo, 2010; Leng et al., 2009d). Typical electroactive polymers include silicone and polydimethylsiloxane (PDMS).

In contrast to most other studies, the compliant substrates investigated in this paper are shape-memory polymers (Lv et al., 2010; Lu et al., 2010; Lan et al., 2009; Leng et al., 2008, 2009a,b,c, 2011; Leng and Du, 2010; Yu et al., 2011). SMPs can undergo significant macroscopic deformation upon the application of various external stimulus (e.g., heat, electricity, light, magnetism, moisture and even changes in pH) (Leng et al., 2011).

The shape-memory cycle of a fibre-reinforced SMPC can be described as follows: first, raise the temperature of the laminate to the glass transition temperature of the material. Then, bend the laminate along a cylindrical surface and constrain it to remain bent. While the shape of the laminate is held, lower the temperature until it falls below the glass transition temperature of the polymer. After the laminate is hardened, remove the constraint. As a result, the laminate will keep the deformed shape, and it will not revert spontaneously. Finally, heat the laminate again to realise the deployable characteristic of the structure, which will return to the original shape (Lan et al., 2009; Lv et al., 2010; Yu et al., 2011; Leng et al., 2011; Leng and Du, 2010). For the strong restraint of the cylinder during the deformation process, the fibres in the surface act as a deformation feature, with shearing-buckling as the main deformation mode. The buckled or wavy configurations can be stretched and compressed in a nondestructive way, similar to the physics of the motion of an accordion bellows.

A fibre-reinforced fabric SMPC was developed for industrial application (Lan et al., 2009; Leng et al., 2009a, 2011; Leng and Du, 2010). The bending recovery force of this SMP-based laminate was larger than those of pure SMP sheets for any given recovery time (Lu et al., 2010; Leng et al., 2009a,b,c). Fibres in SMPs can offer significant improvement in strength, stiffness and resistance against relaxation and creep, thereby providing better mechanical properties. As both functional and structural materials, these SMPs had shown superb potential in many advanced applications (Leng et al., 2009a, 2011; Leng and Du, 2010). For instance, when used as actuator materials, they require no moving parts. Consequently, the use of fibre-reinforced SMPC to produce deployable structures, including antennas, trusses and solar arrays, has attracted considerable interests (Lan et al., 2009; Leng and Du, 2010; Leng et al., 2011).

The local and global buckling analysis of film/compliant substrate systems, as well as nanotube or nanowire/compliant substrate systems, have been the topics of broad research interests recently (Cerda and Mahadevan, 2003; Chen and Hutchinson, 2004; Huang et al., 2004, 2005; Huang, 2005; Audoly and Boudaoud, 2008a,b,c; Ryu et al., 2009; Xiao et al., 2010; Cai et al., 2011).

Several recent nonlinear analyses have determined the wavelengths and amplitudes of sinusoidal wrinkles (Chen and Hutchinson, 2004; Huang et al., 2005). Using the finite element method, Chen and Hutchinson have found that the herringbone pattern has the minimum energy of several competing patterns (Chen and Hutchinson, 2004).

These researchers first obtained the amplitude and wavelength of the sinusoidal wrinkles as functions of the modulus and thickness of the substrate. Their results showed that the wavelength of the wrinkles remains constant as the amplitude of the wrinkles increases. They also developed a spectral method to evolve two-dimensional patterns of wrinkles and represent the exact three-dimensional elastic field of the substrate in Fourier space (Huang et al., 2005).

The emergent nonlinear properties of the buckling behaviours of some of the periodic modes were also elucidated (Audoly and Boudaoud, 2008a,b,c).

Researchers established a continuum mechanics theory for the in-surface buckling of one-dimensional nanomaterials on compliant substrates, and simple analytical expressions were obtained for the buckling wavelength, amplitude and critical buckling strain in terms of the bending and tension stiffness of the nanomaterial and the matrix elastic properties (Xiao et al., 2010).

Further aspects of the nonlinear post-buckling behaviour of a film/substrate system were explored by employing an analytical upper-bound calculation and numerical finite element analysis to determine the relationship between the observed periodic patterns and the level of overstress noted in the next section (Cai et al., 2011).

Based on the analytical method in the Refs. Huang et al. (2005), Chen and Hutchinson (2004), Jiang et al. (2008), Barrett et al. (2006), Francis et al. (2007) and Ryu et al. (2009), this paper developed an improved analysis method of the mechanics of the in-surface buckling for fibre-reinforced SMPC. Similar to the study of the normal buckling of stiff thin films and single wall nanotubes on compliant substrates, the mechanical analysis of in-surface buckling in Section 3 provides an analytical form of the total energy of the system, which consists of the fibre buckling deformation energy, the matrix shear deformation energy in the buckling area and the fibre/matrix tensile deformation energy in the unbuckling area. Furthermore, the analytical expressions for key parameters describing the buckling deformation and local post-buckling mechanics of unidirectional fibre-reinforced SMPC are introduced. These parameters include the critical buckling curvature, the critical buckling position, position of the neutral plane, wavelength of the buckling fibre, amplitude of the buckling fibre and macroscopic strain of the composite material. Additionally, corresponding experiments are conducted to verify the accuracy of the key parameters. The analysis is demonstrated to provide theoretical predictions which are in good agreement with the experimental data.

The fibre-reinforced SMPC with microbuckling can be used for deployable structures in space such as antennas, trusses and solar arrays (Lan et al., 2009; Leng and Du, 2010;

Leng et al., 2011). The methodology in this paper can be extended to analyse similar engineering problems, such as deformation analysis of flexible multilayer printed wiring board used for foldable display. The results of this paper may apply to analyse some failure modes in fibre-reinforced composites under complex loading conditions.

2. The buckling mechanics of fibre-reinforced shape-memory composite materials

Neutral plane in classic mechanics of materials is mostly considered to locate at the middle plane of cross section for isotropic solid. This paper considers the movement of neutral plane and corresponding buckling behaviour of composite materials. In order to achieve the deformation characteristics (critical buckling curvature, critical buckling position, position of the neutral plane, wavelength of the buckling fibres, etc.), the strain state of the cross section for SMPC is divided into three areas: the non-buckling stretching area, non-buckling compression area and buckling compression area. Based on the expressions of strain energy, employing the principle of minimum energy, the distributed deformation characteristics for the entire SMPC is obtained.

2.1. Fundamental equation

The fibre buckling deformation is assumed to have the following sinusoidal shape:

$$y = A\cos\left(\frac{m\pi x}{\lambda}\right) \tag{1}$$

When $m = 1$,

$$y = A\cos\left(\frac{\pi x}{\lambda}\right) \tag{2}$$

where λ denotes the half-wavelength of fibre buckling and A represents the amplitude (Fig. 1). The macroscopic strain along the Y-axis can be expressed as follows:

$$\varepsilon = \frac{\Delta L}{L} = \frac{1}{2L}\int_0^L \left(\sqrt{(dx)^2 + (dy)^2} - dx\right)dx \approx \frac{1}{2L}\int_0^L \left(\frac{dy}{dx}\right)^2 dx \tag{3}$$

Considering Eq. (2), we obtain

$$\varepsilon = \frac{A^2\pi^2}{4\lambda^2} \tag{4}$$

Accordingly, we obtain

$$A = \sqrt{-\varepsilon_{xx}}\frac{2\lambda}{\pi} \tag{5}$$

The in-plane strain, ε_{xx}, can be determined from the following expression:

$$\varepsilon_{xx} = k(z - z_{ns}) \tag{6}$$

Substituting Eqs. (6) and (5) into Eq. (2) yields

$$y = \sqrt{k(z_{ns} - z)}\frac{2\lambda}{\pi}\cos\left(\frac{\pi x}{\lambda}\right) \tag{7}$$

Assuming that both the fibre and the shape-memory material matrix are linearly elastic materials, the strain energy expression of an infinitesimal body element ΔV can be expressed as follows:

$$\begin{aligned}\Delta U_T &= 1/2\sigma_{ij}\varepsilon_{ij}\Delta V \\ &= 1/2(\sigma_{xx}\varepsilon_{xx} + \sigma_{yy}\varepsilon_{yy} + \sigma_{zz}\varepsilon_{zz} + \tau_{xy}\gamma_{xy} + \tau_{xz}\gamma_{xz} \\ &\quad + \tau_{yz}\gamma_{yz})\Delta V\end{aligned} \tag{8}$$

The main factor to be considered in the bending deformation of an SMPC is the strain ε_{xx} along the circle direction, while the longitudinal strain ε_{yy} and the radial strain ε_{zz} are relatively small and can be ignored. Additionally, considering the rigidity constraint boundary condition in the Y–Z plane and neglecting the shear strain γ_{xz} in the X–Z plane, Eq. (8) can be simplified to the following expression:

$$\Delta U_T = \Delta U_{xx} + \Delta U_{xy} + \Delta U_{xz} \tag{9}$$

in which

$$\begin{aligned}\Delta U_{xx} &= 1/2\sigma_{xx}\varepsilon_{xx}\Delta V \\ \Delta U_{xy} &= 1/2\tau_{xy}\gamma_{xy}\Delta V \\ \Delta U_{xz} &= 1/2\tau_{yz}\gamma_{yz}\Delta V\end{aligned} \tag{10}$$

In addition, the buckling strain energy of the fibre must be considered, in addition to its buckling deformation energy (ΔU_f must be added to ΔU_T).

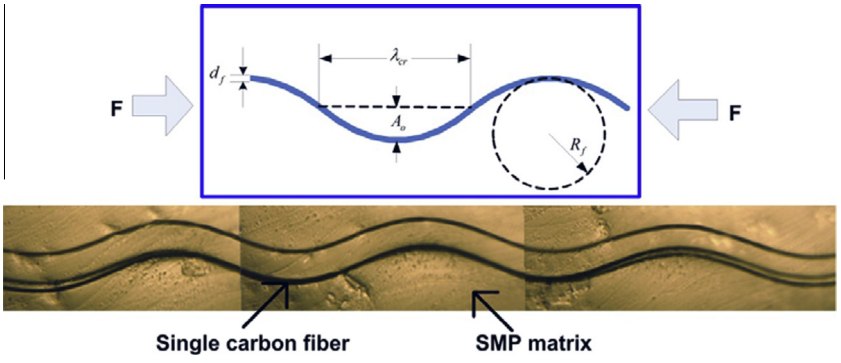

Fig. 1. The post-microbuckling of the fibre-reinforced shape-memory polymer composite under compressive loading (R_f curvature radius; λ_{cr} buckling wavelength; A_o buckling amplitude; d_f diameter of fibre).

$$\Delta U_T = \Delta U_{xx} + \Delta U_{xy} + \Delta U_{yz} + \Delta U_f \quad (11)$$

Based on the analytical method in the Refs. Huang et al. (2005), Chen and Hutchinson (2004), Barrett et al. (2006), Francis et al. (2007) and Ryu et al. (2009), etc., the methodology in this paper is improved, and accordingly the total energy expression U_T is made up with the following energetic subentries for different deformation models of the material:

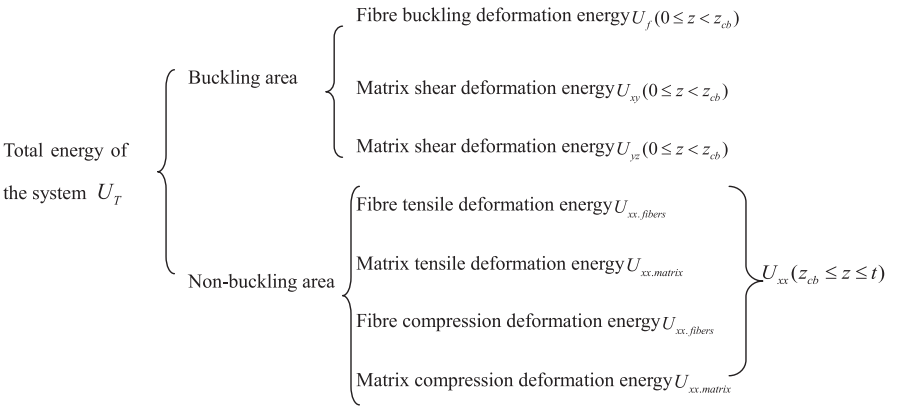

maintained while the temperature is lowered until it falls below the glass transition temperature; then, the restraint is removed after the laminate is hardened. Eventually, the laminate will retain the deformation shape without reverting (as Fig. 2b). By heating the laminate again, the structure can be deployed, causing it to recover its original shape (Fig. 2c). The ability of materials to maintain their deformation shapes is a key factor in the shape-memory effect.

2.2. Problem descriptions

The shape-memory cycle thermodynamics of the fibre-reinforced SMPC occurs as follows: First, the material is heated to its glass transition temperature. Then, the planar composite material laminate bends (Fig. 2a) along the cylindrical surface of a radial cylinder. The constraint is

To provide strong restraint of the cylinder during the deformation process, fibres are included as deformation features in the laminater surface (Fig. 2d), and deformation occurs by shear buckling.

A long and thin columnar carbon fibre has a tensile strength far greater than its compressive strength. The tensile strength is also greater than the shear strength of the

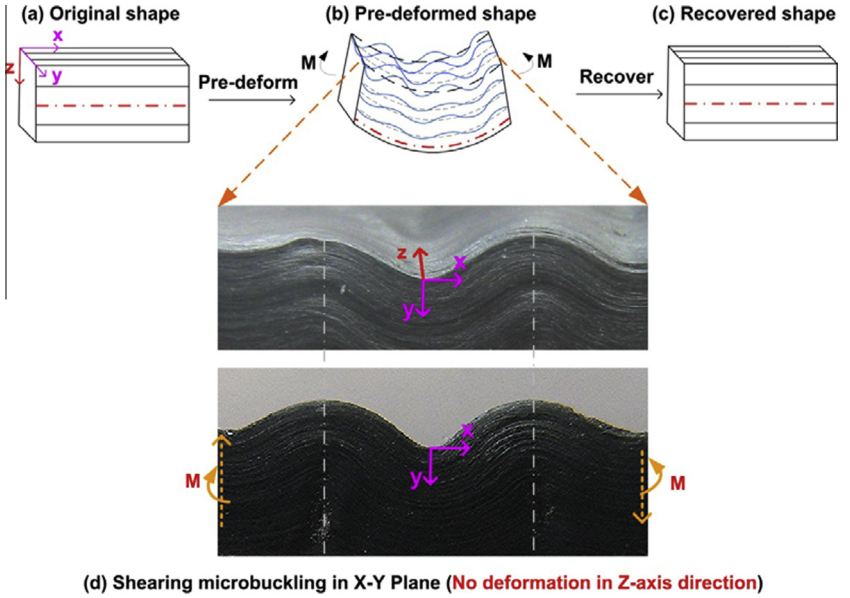

Fig. 2. The in-plane (X–Y plane) deformation of the fibre-reinforced SMP composite (no deformation in the Z direction, mode of buckling is the shear mode).

resin matrix. During the bending deformation process of a fibre-reinforced SMPC, the shear stiffness of the matrix under compression is not adequate to support the lateral deformation of the fibre; consequently, the fibre will buckle as a result of instability.

The expansion process of a fibre-reinforced SMPC is equivalent to the process from state b to state c. On the other hand, the transition from state a to state b and from state b to state c are reversal deformation processes (ignoring the energy lost in the storage of strain energy). In order to understand this process more easily, this paper only considers the deformation process from state a to state b. In this process, there are 4 basic parameters of interest in the buckling deformation of fibre-reinforced SMPC.

1 The critical buckling position. During the bending process, as the curvature increases, there is no buckling at first; the material begins to buckle when the curvature reaches a certain (critical) value.
2 The neutral plane position. During the buckling process (as curvature increases gradually), when the curvature reaches a certain value, the neutral plane gradually moves to the outboard tensile side of the cross section from the symmetry mid-plane.
3 Wavelength of fibre buckling.
4 Amplitude of fibre buckling. The value of the fibre buckling amplitude is not a constant along the thickness direction (Z axis). With a fixed curvature, the amplitude of the flexural wave reaches its maximum in the interior uncompressed surface and declines along the thickness direction until it reaches the critical buckling plane and the amplitude becomes zero (no buckling).

Furthermore, the problem is three-dimensional. In the X–Y plane, the fibre deformation is described by the shearing model, and the energy of the system is related to the X (length direction) and Z (thickness direction) coordinates. Meanwhile, the wavelength of the buckling fibre and other parameters are related to the X (length direction) and Z (thickness direction) coordinates.

Finally, concerning the structure of the SMPC, the principal way to improve the driving force of laminate deployment without changing the material properties is to increase the thickness of the material (the width is fixed, and material failure occurs at smaller bending curvatures). In the optimal design of the material, the relationship between the thickness, curvature and failure strain must be considered.

3. The thermodynamic system energy of shape-memory composite materials

As shown in Fig. 3, the cross section of the composite material under a bending moment can be zoned into three areas: the non-buckling stretching area, the non-buckling compression area and the buckling compression area. These areas are defined by three variables: the critical buckling position z_{cb}, the neutral plane position z_{ns} and the fibre buckling half-wavelength λ.

As Fig. 3a shows, at the glass transition temperature ($T = T_g = 100\ ^\circ C$), a bending moment is applied along the positive direction of the Y axis. In the bending process, the curvature increases gradually from zero. Once the curvature increases beyond the critical value k_c, the fibre begins to buckle at the $z = 0$ position. The boundary line can be expressed as z_{cb} (critical bending). The neutral surface moves towards the outside tensile surface along the Z axis from the original position and stops when it reaches the equilibrium position. As Fig. 3b shows, in the area where $0 \leqslant z < z_{cb}$, the material bears a compression strain, and the fibre undergoes buckling; in the area where $z_{cb} < z < z_{ns}$, the material experiences compression strain without fibre buckling and in the area where $z_{ns} < z \leqslant t$, the material exhibits tensile strain. Plastic deformation, failure of the matrix and failure of the fibre will not be considered in this process.

3.1. Fibre buckling strain energy U_f

The bending of a buckling beam with a small strain and a large displacement can be described by the buckling strain energy equation of a single fibre with length l as follows:

$$U_{f(\text{single fibre})} = \frac{1}{2} E_f I_f \int_0^l \left(\frac{d^2 y}{dx^2}\right)^2 dx \tag{12}$$

Inserting equation (7) into equation (12), we can obtain

$$U_{f(\text{single fibre})} = \frac{E_f I_f l k \pi^2 (z_{ns} - z)}{\lambda^2} \tag{13}$$

In the Y direction (on a cylindrical surface with a specific radius), all of the fibre buckling deformation models are identical, and the equivalent strain energy per unit length in Y direction can be described as follows:

$$U_{f\ (\text{one layer})} = \frac{w}{h} U_{f\ (\text{single fibre})} \tag{14}$$

where h denotes the distance between the centres of the adjacent fibre circles.

Supposing that the fibre deformation is the same throughout the X–Y plane, the fibre deformation energy along Z axis is

$$U_f = \sum_{n=1}^{m} \frac{w}{h} \frac{E_f I_f l k \pi^2}{\lambda^2} (z_{ns} - nh) \tag{15}$$

where h is the distance between the centres of the circles of adjacent fibres, $n = 1, 2, 3 \ldots m$, $m = z_{cb}/h$, and m is an integer. Then we can obtain:

$$U_f = \frac{w E_f I_f l k \pi^2}{2\lambda^2 h^2} z_{cb} (2 z_{ns} - z_{cb} - h) \tag{16}$$

The equation above can be simplified as follows:

$$U_f = \frac{w E_f I_f l k \pi^2}{2\lambda^2 h^2} z_{cb} (2 z_{ns} - z_{cb}) \tag{17}$$

The volume of a fibre, v_f, satisfies the expression of $v_f = [\pi (d/2)^2]/h^2$. Substituting this expression into Eq. (17) yields the following:

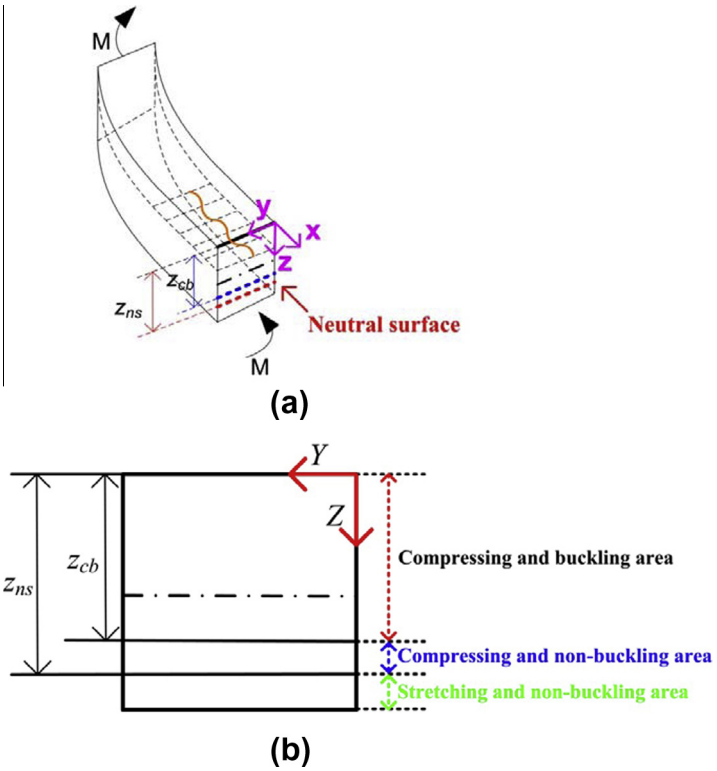

Fig. 3. Illustration of bending deformation of the fibre-reinforced SMP composite, (a) illustration of SMPC shell, (b) strain state of cross-section.

$$U_f = U_f(z_{cb}, z_{ns}, \lambda) = \frac{2wlk\pi v_f E_f I_f}{\lambda^2 d^2} z_{cb}(2z_{ns} - z_{cb}) \quad (0 \leqslant z_{cb} < z_{ns} < t) \tag{18}$$

It should be noted that, for the material strain of the buckling fibre itself, the curvature of the fibre-reinforced material $\tilde{k}$ is

$$\tilde{k} = \frac{|y''|}{(1+y'^2)^{3/2}} \tag{19}$$

Substituting equation (3) into (19), we obtain

$$\tilde{k} = \frac{\left|\frac{A\pi^2}{\lambda^2}\cos\left(\frac{\pi x}{\lambda}\right)\right|}{\left[1+\frac{A^2\pi^2}{\lambda^2}\sin^2\left(\frac{\pi x}{\lambda}\right)\right]^{3/2}} \tag{20}$$

Obviously, when $x = n\lambda, (n = 1, 2, 3\ldots)$, corresponding to the maximum curvature of the carbon fibre monofilament $\tilde{k}$, the maximum material strain $\tilde{\varepsilon}_{\max}$ can be calculated as follows:

$$\tilde{\varepsilon}_{\max} = \frac{dA\pi^2}{2\lambda^2} \tag{21}$$

From the experimental and theoretical results (see Table 4), the maximum bending curvature of the SMPC investigated in this paper is 50 m^{-1}, and the corresponding fibre strain and geometric deformation are the maximum values of the material parameters. Here, we only consider the situation in which k equals 50 m^{-1}. Inserting the experimental results shown in Table 4 into Eq. (20), we determine that the curvature $\tilde{k}$ of the carbon fibre is 1328 m^{-1}; furthermore, the maximum stretching/compression strain is 0.48% (fibre diameter d = 7 um, the neutral surface is on the middle plane of the carbon fibre). From these parameters, it shows that the geometric displacement of the structure is large in the buckling process of the fibre, while the strain in the material itself is small. This problem is typical of large macroscopic structural displacements with small materials strains. Thus, the buckling equation (13) is reasonable. When k is smaller than 50 m^{-1}, the fibre material curvature $\tilde{k}$ and the strain becomes smaller.

For large-displacement geometric deformations of the buckling fibre, the residual will be on the order of magnitude of $(A/\lambda)^2$ when using the buckling equation (13) to calculate the deformation energy. Furthermore, we consider the circumstance in which k = 50 m^{-1}. Using the results of Table 4, we determine the largest residual of the buckling equation (13) to be approximately 3.9%. For k less than 50 m^{-1}, the residual is smaller; consequently, we do not consider the geometrical non-linearity caused by structure displacement during the loading procedure.

In conclusion, when using the buckling equation, the problem investigated in this paper is characterised by minimal materials strain and large structural displacement; as a result, the non-linearity of the material can be ignored. In addition, the malformation gratitude of the flexure deformation is small, and it is unnecessary to consider the geometric non-linearity. Eq. (13), therefore, is reasonable.

3.2. Shearing strain energy U_{xy} of the matrix

During the bending deformation process of the SMPC, the deformation along the circumferential direction of the bending cylinder is restricted by complete restraint. There is no deformation along Z axis (displacement along the circle of $u = 0$, longitudinal displacement $v \neq 0$). Thus, we consider the shearing deformation but ignore the shearing strain γ_{xz} in the X–Z plane because the shear modulus of fibre is much larger than that of the shape-memory polymer matrix. Under the assumption of equal stress, the shearing strain energy of the fibre is much smaller than that of the matrix. As a result, we ignore the fibre shearing strain energy, and the buckling half-wavelength and amplitude of the fibre in the X–Y plane remain constant. Then, the shearing strain of the matrix can be expressed as follows:

$$\gamma_{xy} = \frac{\partial v}{\partial x} + \frac{\partial u}{\partial y} = \frac{\delta y}{\delta x} = -2\sqrt{k(z_{ns} - z)}\sin\left(\frac{\pi x}{\lambda}\right) \tag{22}$$

in which $\gamma_{xy}(x, z)$ is independent of y. Additionally, U_{xy} only exists in the compression buckling section. The integrating range along the Z direction extends from the inside compression surface to the neutral surface z_{ns}, and the composite material is simplified into a parallel monolayer board divided by matrix. In the X–Z plane, we obtain the following expression:

$$U_{xy} = \frac{1}{2}\int_0^{z_{cb}}\int_0^{w}\int_0^{l} v_m G_m \gamma_{xy}^2 dxdydz \tag{23}$$

Equation (22) can be substituted into (23)

$$U_{xy} = U_{xy}(z_{cb}, z_{ns}) = \frac{v_m G_m lwk}{2} z_{cb}(2z_{ns} - z_{cb}) \quad (0 \leqslant z_{cb} < z_{ns} < t) \tag{24}$$

3.3. Shearing strain energy U_{yz} of the matrix

During the bending deformation process of SMPC, the radial deformation of the bending cylinder is completely restrained and there is no displacement in the Z direction (a radial displacement of $w = 0$ and a longitudinal displacement $v \neq 0$), so that we ignore the shearing strain in the X–Z plane, γ_{xz} when considering the shearing deformation. Along the Z direction, the buckling amplitudes of the fibres differ. Thus, there exists a shearing deformation between any two nearest neighbour fibres in the Y–Z plane, and the shearing strain of the matrix in this plane can be expressed as follows:

$$\gamma_{yz} = \frac{\partial w}{\partial y} + \frac{\partial v}{\partial z} = \frac{\delta y}{\delta z} = \frac{k\lambda}{\pi\sqrt{k(z_{ns} - z)}}\cos\left(\frac{\pi x}{\lambda}\right) \tag{25}$$

where $\gamma_{yz} = \gamma_{yz}(x, z)$, which is completely independent of coordinate y. The composite material is simplified into a parallel monolayer board which is divided by matrix, and the strain energy U_{yz} of the X–Y plane can be calculated as follows:

$$U_{yz} = \frac{1}{2}\int_0^{z_{cb}}\int_0^{w}\int_0^{l} v_m G_m \gamma_{yz}^2 dxdydz \tag{26}$$

The following integrated expression is obtained:

$$U_{yz} = U_{yz}(z_{ns}, z_{cb}, \lambda) = \frac{lwk v_m G_m \lambda^2}{4\pi^2}\ln\left(\frac{z_{ns}}{z_{ns} - z_{cb}}\right) \tag{27}$$

3.4. Stretching and compression strain energy U_{xx} of the fibre and matrix

U_{xx} includes two parts, the stretching strain energy of the tensile area ($z_{ns} \leqslant z \leqslant t$) in the matrix and the fibre and the compression strain energy of the compression area ($z_{cb} < z < z_{ns}$) in the matrix and fibre, while it does not include the bending strain energy of the buckling fibre ($0 \leqslant z < z_{cb}$ area). For the matrix and fibre are of simple stretching or compression strain state, we can determine the total strain energy of the matrix and fibre according to the parallel connection model of the composite material using the assumption of equal strain. U_{xx} only exists in the non-buckling area of stretching or compression, and for an integrating range along the Z direction from z_{cb} to the outside compression plane, we obtain the following equation:

$$U_{xx} = \frac{1}{2}\int_{z_{cb}}^{t}\int_0^{w}\int_0^{l} E_{xx}\varepsilon_{xx}^2 dxdydz \tag{28}$$

Inserting equation (7) into (28), we get

$$U_{xx} = \frac{lwk^2(v_m E_m + v_f E_f)}{6}\left[(t - z_{ns})^3 + (z_{ns} - z_{cb})^3\right] \tag{29}$$

in which E_m is the stretching/compression modulus of the matrix and E_f is the stretching/compression modulus of the fibre (non-buckling).

According to Fig. 4, approximately 50% of the shape-memory material strain range belongs to the linear-elastic deformation, in which the strain in the stretching area of the polymer is small from Eq. (40), we can determine that the maximum strain in the stretching area is 0.44% when $k = 50\ \mathrm{m}^{-1}$ and we ignore the plastic deformation of the materials. Additionally, the maximum strain for carbon fibre in the system is less than 1.5%; consequently, we only consider the linear-elastic constitutive relation.

3.5. Total energy of the system

By substituting all of the energy expressions (U_{xx}, U_{xy}, U_{yz}, U_f) into the expression for the total energy U_T, we obtain the following expression:

$$\begin{aligned} U_T &= U_T(z_{ns}, z_{cb}, \lambda) \\ &= \frac{lwk^2(v_m E_m + v_f E_f)}{6}\left[(t - z_{ns})^3 + (z_{ns} - z_{cb})^3\right] \\ &\quad + \frac{v_m G_m lwk}{2} z_{cb}(2z_{ns} - z_{cb}) + \frac{lwk v_m G_m \lambda^2}{4\pi^2} \\ &\quad \times \ln\left(\frac{z_{ns}}{z_{ns} - z_{cb}}\right) + \frac{2wlk\pi v_f E_f I_f}{\lambda^2 d^2} z_{cb}(2z_{ns} - z_{cb}) \end{aligned} \tag{30}$$

In this paper, the fibre-reinforced SMPC structure has the following material parameters: length, $l = 30$ mm; width, $w = 5$ mm; thickness, $t = 2$ mm; diameter of the carbon fibre (T300), $d = 7$ um; $E_f = 230$ GPa. The Young's

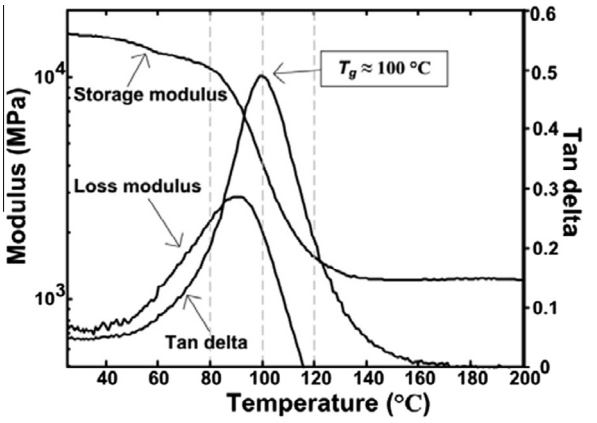

Fig. 4. DMA test of fibre-reinforced SMP composite.

modulus and shear modulus of the SMPs near their glass transition temperature are $E_m = 14$ MPa and $G_m = 5$ MPa, so that $v_m G_m/(v_m E_m + v_f E_f) = 8.69 \times 10^{-5}$. Unless defined otherwise, the curvature of the SMPC is $k = 50\ \mathrm{m}^{-1}$, producing a radius of curvature equal to 20 mm. By investigation, we determined that there exists a nadir in the system energy (discussed in detail in later chapters) at a half-wavelength of approximately 1.0–1.5 mm and a neutral surface relative position of approximately 0.85–0.97. According to the energy method, we can determine the arrest point of the structure energy and compute the main parameters of the balanced system (neutral surface position, critical buckling position, buckling fibre half-wavelength, etc.).

The energy components in Eq. (30) exist in different areas of the laminate; for example, U_{xx} represents the strain energy of the non-buckling fibre and the matrix stretching/compression area, U_{xy} is the shearing energy of the matrix buckling area in the X–Y plane, U_{yz} is the shearing energy of the matrix buckling area in the Y–Z plane, and U_f is the deformation energy of the buckling area of the fibre. The energy is calculated independently, without consideration of the coupling effect.

4. Analysis expression of key parameters

4.1. Buckling critical point and displacement of the neutral surface

This paper introduces the notion of the non-buckling compression area and adopts a self-consistent calculation to solve Eq. (29). Similar to the solution of Eq. (30), we ignore U_{yz} and U_f when solving z_{ns} and z_{cb}.

$$\begin{aligned}\tilde{U}_T &= U_T(z_{ns}, z_{cb}) \\ &= \frac{lwk^2(v_m E_m + v_f E_f)}{6}\left[(t - z_{ns})^3 + (z_{ns} - z_{cb})^3\right] \\ &\quad + \frac{v_m G_m lwk}{2} z_{cb}(2z_{ns} - z_{cb})\end{aligned} \tag{31}$$

Through the energy method, we obtain $\tilde{U}_T$, which is the system of partial differential equations defining z_{ns} and z_{cb}

$$\begin{cases} \frac{\partial \tilde{U}_T(z_{ns}, z_{cb})}{\partial z_{cb}} = 0 \\ \frac{\partial \tilde{U}_T(z_{ns}, z_{cb})}{\partial z_{ns}} = 0 \end{cases} \tag{32}$$

According to Eq. (32), we obtain the following results:

$$z_{cb} = t - \frac{1}{k}\frac{v_m G_m}{v_m E_m + v_f E_f}\left(\sqrt{1 + \frac{2kt}{\frac{v_m G_m}{v_m E_m + v_f E_f}}} + 1\right) \tag{33}$$

$$z_{ns} = t - \frac{1}{k}\frac{v_m G_m}{v_m E_m + v_f E_f}\left(\sqrt{1 + \frac{2kt}{\frac{v_m G_m}{v_m E_m + v_f E_f}}} - 1\right) \tag{34}$$

Further, we obtain the relationship between z_{ns} and z_{cb}:

$$z_{cb} = z_{ns} - \frac{2}{k}\frac{v_m G_m}{v_m E_m + v_f E_f} \tag{35}$$

Inserting (33) into (29) we get

$$\begin{aligned}\hat{U}_T &= U_T(z_{ns}, \lambda) \\ &= \frac{lwk^2(v_m E_m + v_f E_f)}{6}\left[(t - z_{ns})^3 + \frac{8}{k^3}\left(\frac{v_m G_m}{v_m E_m + v_f E_f}\right)^3\right] \\ &\quad + \frac{v_m G_m lwk}{2}\left[z_{ns}^2 - \frac{4}{k^2}\left(\frac{v_m G_m}{v_m E_m + v_f E_f}\right)^2\right] \\ &\quad + \frac{lwk v_m G_m \lambda^2}{4\pi^2}\ln\left(\frac{z_{ns}k}{2\frac{v_m G_m}{v_m E_m + v_f E_f}}\right) \\ &\quad + \frac{2wlk\pi v_f E_f I_f}{\lambda^2 d^2}\left[z_{ns}^2 - \frac{4}{k^2}\left(\frac{v_m G_m}{v_m E_m + v_f E_f}\right)^2\right]\end{aligned} \tag{36}$$

Comparing the first two items and the last two items to see which is smaller. The relationship between the energy and the positions of the neutral surface under different matrix shear modules are shown in Fig. 5 ($G_m = 5$, 10 and 20 MPa) for the composite material with a half-wavelength of $\lambda = 1.25$ mm and a thickness of $t = 2$ mm. The result shows that the curves of $U_{xx} + U_{xy}$ and $U_{xx} + U_{xy} + U_{yz} + U_f$ are nearly parallel, and the first two items $U_{xx} + U_{xy}$ are much greater than $U_{yz} + U_f$.

Similarly, Fig. 6 shows the relationship between the energy and the position of the neutral surface under different curvature conditions. The result still indicates that the $U_{xx} + U_{xy}$ and $U_{xx} + U_{xy} + U_{yz} + U_f$ curves are nearly parallel, and $U_{xx} + U_{xy}$ is much larger than $U_{yz} + U_f$. Consequently, it is reasonable to replace $U_{xx} + U_{xy} + U_{yz} + U_f$ by $U_{xx} + U_{xy}$ in (36). Therefore, the adoption of the self-consistent calculation to solve equation (29) is valid.

Equations (33) and (34) also need to satisfy the condition of $0 \leqslant z_{cb} < z_{ns} < t$. This paper studies the control of displacement (the control of curvature) rather than the control of force. The energy method is used to determine the position of the neutral surface z_{ns} and the curving half-wavelength λ when the curvature k is fixed. This approach means that k defines a boundary condition rather than acting as a variable. Then, we can discuss the relationship between z_{ns}, z_{cb} and k.

First, under the condition that $z_{cb} \geqslant 0$, Eq. (33) provides the following relationship:

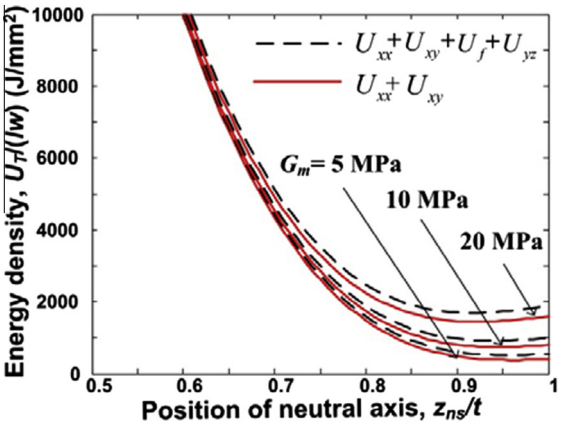

Fig. 5. Energy-z_{ns}/t relationship at different matrix shear modulus (G_m = 5, 10, and 20 MPa, k = 50 m^{-1}).

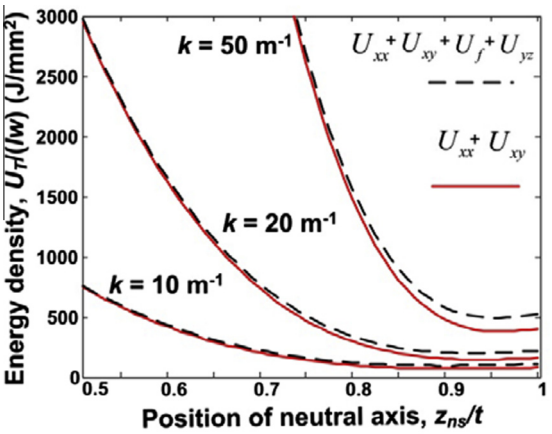

Fig. 6. Energy-z_{ns}/t relationship at different curvatures (k = 10, 50, and 100 m^{-1}, G_m = 50 MPa).

$$k \geqslant \frac{4}{t}\frac{v_m G_m}{v_m E_m + v_f E_f} \tag{37}$$

Inserting (37) into (34), we obtain the following:

$$\frac{z_{ns}}{t} \geqslant \frac{1}{2} \tag{38}$$

Obviously, when $z_{cb} = 0$, there is no fibre curvature in the material; when $z_{cb} > 0$, fibre curvature occurs and the critical curvature k_c is obtained.

$$k_c = \frac{4}{t}\frac{v_m G_m}{v_m E_m + v_f E_f} \tag{39}$$

Under this condition, the position of the neutral surface is $z_{ns}/t = 1/2$, proving that the neutral surface of the initial material position is at the middle of the plane. When the curvature increases from infinitesimal ($k = 1/\rho \to 0$) to some critical curvature, the fibre in the material begins to curve. The critical curvature of the general material is greater, so the material is destroyed before the fibre buckles; we cannot observe the phenomenon of curvature and the neutral surface does not move.

The shear modulus of the SMP examined in this paper is lower at the glass transition temperature; thus, the neutral plane moves when the curvature is greater. Physically, the position of the neutral surface and its movement are determined by the equilibrium relationship of U_{xx} and U_{xy}, meaning that when the former increases monotonically, the latter decrease monotonically, and the minimum energy equilibrium point can be deduced from the sum of the two terms.

Also, the critical strain ε_c of the material is expressed as follows:

$$\varepsilon_c = \frac{2 v_m G_m}{v_m E_m + v_f E_f} \tag{40}$$

In summary,

$$\varepsilon_{xx} = \begin{cases} 0 & (k \leqslant k_c) \\ t - \frac{1}{k}\frac{v_m G_m}{v_m E_m + v_f E_f}\left(\sqrt{\frac{1+\frac{2kt}{v_m G_m}}{v_m E_m + v_f E_f}}+1\right) & (k > k_c) \end{cases} \tag{41}$$

$$\varepsilon_{xx} = \begin{cases} \frac{t}{2} & (k \leqslant k_c) \\ t - \frac{1}{k}\frac{v_m G_m}{v_m E_m + v_f E_f}\left(\sqrt{\frac{1+\frac{2kt}{v_m G_m}}{v_m E_m + v_f E_f}}+1\right) & (k > k_c) \end{cases} \tag{42}$$

Furthermore, we discuss the case in which $z_{cb} < z_{ns}$. From (35), we can see that z_{cb} is always smaller than z_{ns}. It is also clear that z_{cb} and z_{ns} are smaller than t.

The variation of the critical curvature and neutral surface positions during the buckling process are shown in Fig. 7. For a material with $M = v_m G_m/(v_m E_m + v_f E_f)$, the fibre curvature appears at the inner buckling side of the material when the value of the curvature increases to k_c. The initial position values, $z_{cb} = 0$ and $z_{ns} = t/2$, increase with the curvature, and z_{cb} and z_{ns} move towards the outside plane when tensile stress is applied.

Additionally, z_{cb} rapidly approaches z_{ns}. This convergence means that the compressing non-buckling area widens from its initial value, and $t/2$ decreases to zero gradually. Fig. 7 shows that the properties of composite materials (different values of $v_m G_m/(v_m E_m + v_f E_f)$) vary with the properties of the neutral surface. This trend is treated in detail in Fig. 8.

Plug Equation (39) into $\varepsilon_{xx} = k(z - z_{ns})$, we obtain the macro-strain of the SMP lamina along X axis

$$\varepsilon_{xx} = \begin{cases} Pk(z - \frac{t}{2}) & (k \leqslant k_c) \\ (z - t)k + \frac{v_m G_m}{v_m E_m + v_f E_f}\left(\sqrt{\frac{1+\frac{2kt}{v_m G_m}}{v_m E_m + v_f E_f}}-1\right) & (k > k_c) \end{cases} \tag{43}$$

From Fig. 8, we can determine the variation of the maximal strain of the inner compressing side ($z = 0$) during the process of bending (as the curvature increases gradually).

Table 1 gives different critical curvature values k_c (t = 2 mm) based on different material constants $M = v_m G_m/(v_m E_m + v_f E_f)$. From the table, we can see that greater value of the material constant leads to greater value of the critical curvature. Materials that have greater rigidity are harder to bend. A material is damaged when material constant is too large (as $M > 1 \times 10^{-2}$) and the curvature is less than k_c. In this case, curvature does not appear.

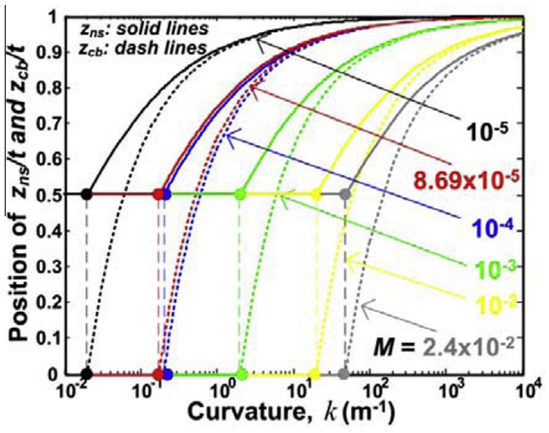

Fig. 7. The relative displacement of the neutral plane and critical buckling position during the bending process (t = 2 mm).

Figs. 7 and 8 and Table 1 discuss the morphing property in the buckling process of the SMP in detail.

At a temperature near the glass transition point and in the case of $k \leqslant k_c$ (G_m has a magnitude of 10 MPa), the SMP does not buckle, the neutral surface always coincides with the section of the symmetrical face, and $\varepsilon_{xx,\max} - kt/2$.

When the curvature increases such that $k > k_c$, the fibres begin to curve and z_{cb} moves away from the inner compressing side. The neutral surface z_{ns} deflects ($z_{ns} > t/2$) during the curve process. The macro-strain can be calculated by Eq. (43). At the glass transition temperature, the Young's modulus of the SMP reached 10–20 MPa, the shear modulus reached 3–7 MPa, the modulus of the carbon fibre became 3∼7 MPa, the fibre volume is 10–30%, and the magnitude of $M = v_m G_m/(v_m E_m + v_f E_f)$ approximated 1×10^{-4}.

Because the critical strain is very small, when the SMP lamina buckles, the neutral surface deflects directly from macro-observing. For instance, the Young's modulus of the fibre-reinforced epoxy polymer shape-memory composite approximates 14 MPa, its shear modulus is 5 MPa, the fibre volume is 20%, and $v_m G_m/(v_m E_m + v_f E_f) = 8.69 \times 10^{-5}$ at the glass transition temperature. In the process of buckling, z_{ns}/t and $\varepsilon_{xx,\max}$ vary along the curve of $v_m G_m/(v_m E_m + v_f E_f) = 8.69 \times 10^{-5}$ in Figs. 7 and 8, respectively.

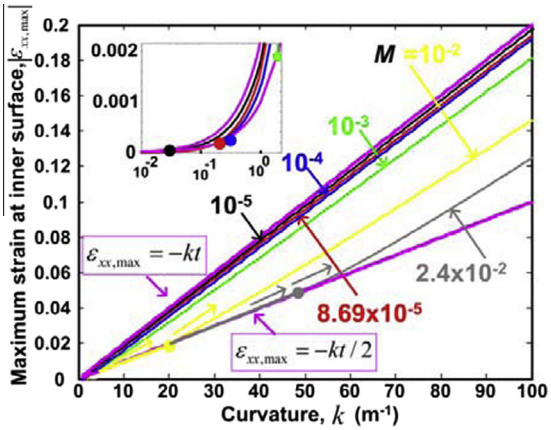

Fig. 8. The maximum strain at the inner compressive surface in the bending process (t = 2 mm).

For the general composite, the neutral surface often has no deflection, and the largest strain of the inner compressive side can be calculated by $\varepsilon_{xx,\max} = -kt/2$. The Young's modulus of the composite matrix approximates 2–5 GPa, its shear modulus approximates 0.5–2 GPa, the modulus of the carbon fibre approximates 230 GPa, the fibre volume is 20%, and the magnitude of $v_m G_m/(v_m E_m + v_f E_f)$ approximates 1×10^{-2}. For the normal fibre-reinforced epoxy polymer shape-memory composite, the resin matrix has a Young's modulus of 3.5 GPa and a shear modulus of 1.4 GPa, the carbon fibre has a modulus of 230 GPa, and $v_m G_m/(v_m E_m + v_f E_f) = 2.43 \times 10^{-2}$.

If we ignore the failure of the material, the neutral surface does not initially move with the increasing curvature ($k \leqslant k_c$), but it still coincides with the section plane of symmetry ($z_{ns}/t = 1/2$). As the curvature increased to k_c = 48.6 - m^{-1}, the neutral surface begun to move towards the outer tensile side. Simultaneously, z_{ns}/t and $\varepsilon_{xx,\max}$vary along the curve of $v_m G_m/(v_m E_m + v_f E_f) = 2.4 \times 10^{-2}$ in Figs. 7 and 8, respectively. When the curvature is equal to 48.6 m^{-1} (t = 2 mm), $\varepsilon_{xx,\max}$ = 4.86%, and the general composite material has already failed. Thus, the fibre-reinforced epoxy polymer shape-memory composite generally has no fibre curvature in practise, and there is no need to consider the motion of the neutral surface.

4.2. The half-wavelength of buckling

Plug the expression of z_{cb} into the energy expressions for U_{xx} and U_{yz} ($k > k_c$), we get the following expressions:

$$U_{yz} = U_{yz}(z_{ns}, \lambda) = \frac{lwkv_m G_m \lambda^2}{4\pi^2} \ln\left(\frac{z_{ns}k}{2\frac{v_m G_m}{v_m E_m + v_f E_f}}\right) \tag{44}$$

$$U_f = U_f(z_{ns}, \lambda) = \frac{2wlk\pi v_f E_f I_f}{\lambda^2 d^2}\left[z_{ns}^2 - \frac{4}{k^2}\left(\frac{v_m G_m}{v_m E_m + v_f E_f}\right)^2\right] \tag{45}$$

The former two items of Eq. (16) (U_{xx} and U_{xy}) do not include λ, while the later two items (U_{yz} and U_f) do include it. Consequently, when the system is in the minimum energy state, only the later two items need to be considered in order to determine the fibre buckling half-wavelength of the system.

$$\hat{U}_T = U_T(z_{ns}, \lambda) = \frac{lwkv_m G_m \lambda^2}{4\pi^2} \ln\left(\frac{z_{ns}k}{2\frac{v_m G_m}{v_m E_m + v_f E_f}}\right) + \frac{2wlk\pi v_f E_f I_f}{\lambda^2 d^2}\left[z_{ns}^2 - \frac{4}{k^2}\left(\frac{v_m G_m}{v_m E_m + v_f E_f}\right)^2\right] \tag{46}$$

The partial differential equation for $\hat{U}_T$, which depends on λ, is determined by the method of energy:

$$\frac{\partial \hat{U}_T(z_{ns}, \lambda)}{\partial \lambda} = 0 \tag{47}$$

Table 1
Critical curvatures of materials with variable material constant (t = 2 mm).

Material constant M[a]	1×10^{-5}	8.69×10^{-5}	1×10^{-4}	1×10^{-3}	1×10^{-2}	2.43×10^{-2}
Critical curvature k_c (m^{-1})	0.02	0.17	0.20	2.00	20.00	48.60
Critical strain ε_c (%)	0.002	0.017	0.020	0.200	2.000	4.860

[a] $M = v_m G_m/(v_m E_m + v_f E_f)$.

Then,

$$A = \begin{cases} +\infty & (k < k_c) \\ \left[\dfrac{8\pi^3 v_f E_f I_f \left(z_{ns}^2 - \frac{4M^2}{k^2}\right)}{v_m G_m d^2 \ln\left(\frac{kz_{ns}}{2M}\right)}\right]^{1/4} & (k \geqslant k_c) \end{cases} \tag{48}$$

$$M = \frac{v_m G_m}{v_m E_m + v_f E_f} \tag{49}$$

Under the condition of the material property ($M = v_m G_m/(v_m E_m + v_f E_f)$), the curvature and thickness are fixed, and the material half-wavelength is independent of coordinate Z, which means that the wavelength is fixed along the direction of thickness.

From Eq. (48), we can determine the relationship for the half-wavelength and curvature under the condition of different thickness. For a material with fixed thickness, as the curvature increases during the process of buckling, the material initially experiences no fibre buckling ($\lambda \to +\infty$). When k increased to k_c, the inner side of the material fibre began to buckle, and λ instantly changed from an infinite to a finite value (λ is discontinuous before and after k_c). According to Fig. 9, when the curvature is greater than 10 m^{-1}, the wavelength remains constant. As the thickness of the material increases, the half-wavelength of buckling increases gradually so that the half-wavelength and the thickness maintain the same.

Table 2 lists the critical curvature and critical half-wavelength of the material under different thickness conditions. As the thickness increases, the critical curvature of the material decreases, the value of the critical strain is fixed (0.017%), and the critical half-wavelength increases. During the bending process, the fibre appears to buckle directly in the experiment because the critical strain is small and it is difficult to observe the process during which the inner side non-buckling state transitions to the buckling state.

$$\lambda_c = \left[\frac{8\pi^3 v_f E_f I_f \left(z_{ns}^2 - \frac{t^2}{4}\right)}{v_m G_m d^2 \ln\left(\frac{2z_{ns}}{t}\right)}\right]^{1/4} \tag{50}$$

Equation (50) defines the relationship between the half-wavelength and the curvature under the condition of different material properties (see Fig. 10).

For a material that has fixed properties, the starting of fibre buckling occurs when the curvature k is larger than k_c. The buckling half-wavelength decreases gradually at the beginning, then becomes flat. As the value of G_m increases, the critical curvature k_c increases, but the stable buckling half-wavelength decreases. For the carbon fibre-reinforced composite, the shear modulus of the matrix clearly affects the buckling of half-wavelength.

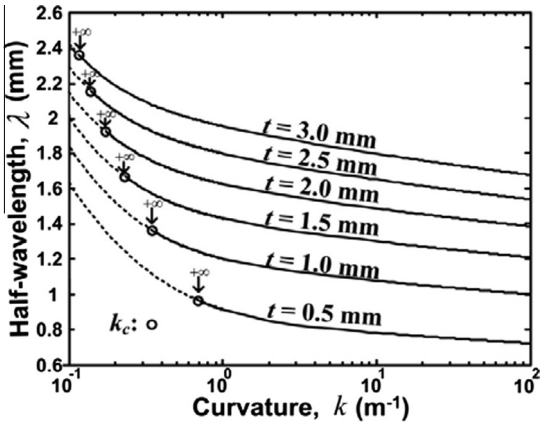

Fig. 9. The relationship of the half-wavelength and curvature for SMP specimens with different thicknesses.

4.3. The material's bulking amplitude

In the area of the composite where compressed micro buckling occurs ($0 \leqslant z < z_{cb}$), the bulking amplitude of the fibre (A) is given by the following:

$$A = \sqrt{-\varepsilon_{xx}}\frac{2\lambda}{\pi} \tag{51}$$

Plug (7) and (48) into (51) we obtain

$$A = \begin{cases} 0 & (k \leqslant k_c) \\ \dfrac{2\sqrt{k(z_{ns}-z)}}{\pi}\left[\dfrac{8\pi^3 v_f E_f I_f \left(z_{ns}^2 - \frac{4M^2}{k^2}\right)}{v_m G_m d^2 \ln\left(\frac{kz_{ns}}{2M}\right)}\right]^{1/4} & (k > k_c) \end{cases} \tag{52}$$

According to the equation above, Fig. 11 shows the distribution of the fibre buckling amplitude during the process of buckling in the direction of thickness. At a fixed curvature, the buckling wavelength gradually increases from the position of z_{ns} to zero along the direction of negative Z axis. Its value is on the order of magnitude of 10^{-4} m. When the curvature increases, the neutral surface moves towards to the outer tensile side, and the amplitude increases gradually at the same time.

Obviously, the fibre buckling wavelength of the SMPC is the greatest at the innermost flexure surface, where it has the following value:

$$A_{\max} = \frac{2\sqrt{kz_{ns}}}{\pi}\left[\frac{8\pi^3 v_f E_f I_f \left(z_{ns}^2 - \frac{4M^2}{k^2}\right)}{v_m G_m d^2 \ln\left(\frac{kz_{ns}}{2M}\right)}\right]^{1/4} \quad (k > k_c) \tag{53}$$

Table 3 lists the critical curvature, critical strain, critical half-wavelength and critical amplitude of the material under different matrix shear modulus conditions. Note that $E_m \ll E_f$; therefore, it is reasonable to ignore the value of E_m.

Table 2
Critical curvatures of materials with variable material constant.

Material thickness t (mm)	0.5	1.0	1.5	2.0	2.5	3.0
Critical curvature k_c (m^{-1})	0.6955	0.3477	0.2318	0.1739	0.1391	0.1159
Critical strain ε_c (%)	0.017	0.017	0.017	0.017	0.017	0.017
Critical half wavelength λ_c (mm)	0.96	1.40	1.70	1.90	2.20	2.40

(G_m = 5 MPa, E_m = 14 MPa, E_f = 230GPa).

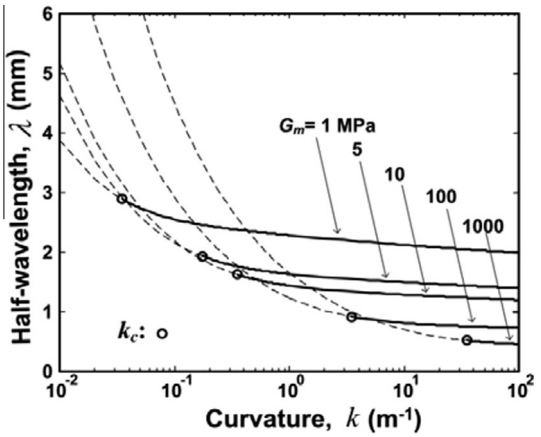

Fig. 10. The relationship of the half-wavelength and curvature for SMP specimens with material property (t = 2 mm).

Figs. 9 and 11 and Table 3 show that the critical curvature, amplitude and strain of the material increase along with system energy, and its critical half-wavelength decreases as the matrix shear modulus increases. As the matrix becomes rigid, the material's fibre becomes much more resistant to buckling. It is difficult to observe general fibre buckling in the composite matrix. It is also difficult to observe the process of the transition from the non-buckling state to the buckling state on the inner compressive side because the critical curvature, critical strain and critical amplitude are small. Thus, the experimental verification of the four critical parameters will not be further discussed in this paper.

5. Theoretical prediction and experimental verification

We have discussed all of the parameters of the theoretical description of the bending-deflection process for a fibre-reinforced shape-memory polymer composite, and we will further verify these parameters with experimental results.

During the buckling process of the fibre-reinforced shape-memory polymer composite (t = 2 mm, $v_m G_m/(v_m E_m + v_f E_f) = 8.69 \times 10^{-5}$) studied in this paper, the relative displacement of the neutral surface z_{ns}/t and the greatest amplitude A_{max} of the inner compressive side ($z = 0$) increase gradually, and the half-wavelength λ decreases initially and then becomes flat (in Fig. 12). The critical curvature k_c is too small to consider. The neutral surface z_{ns}/t and the half wavelength λ approach fixed values of approximately 0.96 and 1.40 mm, respectively, when the curvature is greater than 20 m^{-1} (radius of curvature less than 50 mm).

To verify the above expressions of the key parameters, which come from the theoretical derivation, we prepared a unidirectional carbon fibre-reinforced shape-memory polymer composite lamina and performed a related buckling experiment. The composite was manufactured as follows. A stamping process was utilised to fabricate epoxy SMPC with a carbon fibre volume of approximately 20%. Specific solidification was performed to produce lamina (thickness t = 2 mm), which were cut into strips (30 mm long, 10 mm wide, 2 mm thick). At the glass transition temperature, each sample was curved along a cylinder with a different radius, until the carbon fibre buckled. The strip samples had curvatures of 20, 50, and 100 m^{-1} (the corresponding cylinder radii were 50, 20 and 10 mm, respectively).

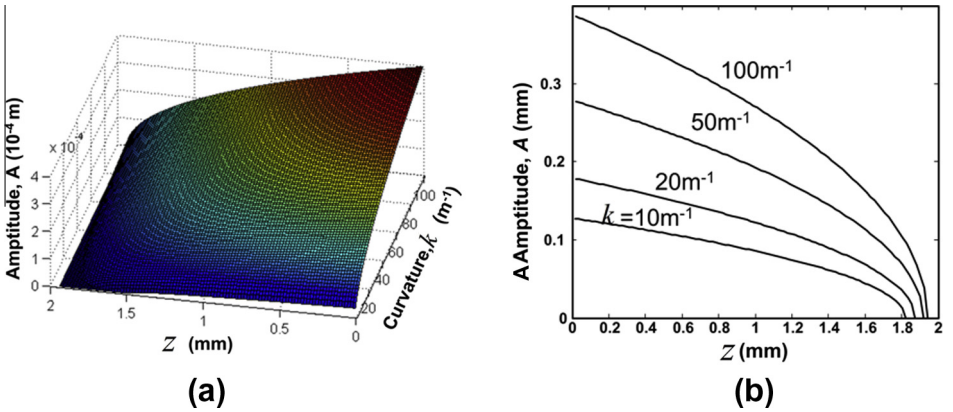

Fig. 11. The evolution of the amplitude and curvature along the thickness direction during the bending process (a) A–z–k, (b) A–z.

Table 3
Critical parameters of materials with variable shear modulus matrix.

Shearing model G_m (MPa)	1	5	10	100	1000
Critical curvature k_c (m^{-1})	0.035	0.174	0.348	3.478	34.774
Critical strain ε_c (%)	0.003	0.017	0.035	0.350	3.470
Critical half wavelength λ_c)(mm)	2.90	1.90	1.60	0.91	0.51
Critical amplitude A_c (mm)	0.010	0.016	0.019	0.034	0.061

(t = 2 mm, E_f = 230GPa).

Table 4
The comparison of theoretical predictions and experimental results for SMP composites at different curvatures.

Curvature k (m^{-1})	Neutral surface Z_{ns}/t	Half wavelength λ (mm)		Maximum amplitude A_{max} (mm)		Macroscopic maximum strain of composite materials ε_{max} (%)		Maximum strain of buckling carbon fibre materials $\tilde{\varepsilon}_{max}$ (%)	
Design value	Theoretical value	Theoretical value	Experimental value	Theoretical value	Experimental value	Theoretical value	Experimental Value	Theoretical value	Experimental value
20	0.936	1.45	1.24 ± 0.05	0.179	0.16 ± 0.02	3.76	4.29 ± 0.91	0.29	0.37 ± 0.04
50	0.959	1.41	1.39 ± 0.11	0.278	0.26 ± 0.02	9.59	8.66 ± 0.80	0.48	0.47 ± 0.05
100	0.971	1.42	–	0.400	–	19.42	–	0.69	–

As shown in Fig. 13, the buckled wave of the carbon fibre was sinusoidal. As the curvature increased, the wavelength remained constant, but the amplitude increased gradually. The white line on the sample shows the measurement position for the wavelength and amplitude, and the measured values are given in Table 4. When the value of the curvature was 20 m^{-1} or 50 m^{-1}, the distributions of the fibre wave and amplitude are regular, and the sample can undergo cyclic straining many times. This paper will later compare the theoretical and experimental results of the fibre wave and amplitude in detail. When the curvature of the material was 100 m^{-1}, the wave shape distribution of buckling fibre was disordered, buckling ruptures of the fibre occurred, and the shape was not able to recover completely. Consequently, the 100 m^{-1} sample will not be utilised in the deployable structure that is discussed later in the paper.

Table 4 gives the theoretical predictions and experimental values of key material parameters under different curvature conditions. The displacement z_{ns} of the neutral surface can be calculated from Eq. (42), and the theoretical value of the half-wavelength λ is calculated by Eq. (48). The greatest amplitude A_{max} of the inner compressive plane (z = 0) is calculated by Eq. (52). The experimental values of the half-wavelength and amplitude are shown in Fig. 11, which displays five values of the wavelength and amplitude of each curvature and the calculation of their

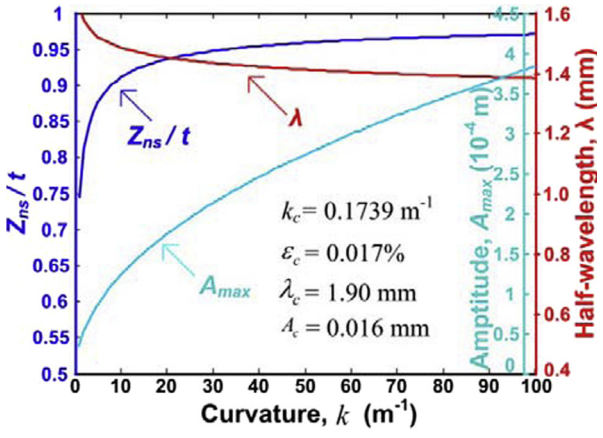

Fig. 12. The theoretical result of a fibre-reinforced SMP composite specimen during the bending process (t = 2 mm, $v_m G_m/(v_m E_m + v_f E_f) = 8.69 \times 10^{-5}$).

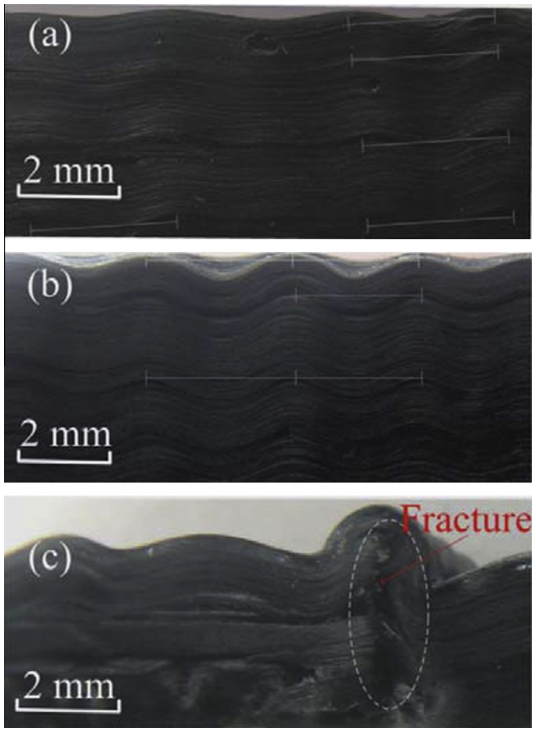

Fig. 13. Microbuckling wavelength at different curvatures (a) 20 m^{-1}, (b) 50 m^{-1}, (c) 100 m^{-1}. The amplitude and wavelength are measured at the position of the white line.

average value and standard deviation. The theoretical value of the macro-compressive strain ε_{max} of the inner compressive plane is calculated by Eq. (43).

According to the measured experimental data for the fibre buckling wavelength and amplitude, we calculated the real macro strain ε_{max} of the inner compressive plane from Eq. (4). The greatest strain $\tilde{\varepsilon}_{max}$ of fibre material itself was determined from Eq. (21), the theoretical values were calculated from the theoretical half-wavelength and maximal amplitude, and the experimental values were obtained from the measured half-wavelength and maximal amplitude.

The limiting stretching and compression strains of the carbon fibre are small, but the curvature of the carbon fibre composite materials utilised in deployable structures must be large. The local post-buckling of the fibre can produce structural bending through large deflection deformations without destroying the material. All of the theoretically predicted parameters and experimental values are completely consistent in order of magnitude, according to Table 4, and the specific results also show good basic agreement. The post-buckling of the carbon fibre produced large macro structural strain (more than 8%) with small material strain (less than 0.5%), and the structure also acquired a large bending curvature($k = 50\ m^{-1}$, $t = 2$ mm). Thus, the fibre small strain produced large geometrical deformation and displacement of the composite structure.

6. Discussions

For the simplification of SMP composites, fibre and SMP matrix is assumed to be as linear elasticity under small deformation at a constant ambient temperature, and therefore the following factors is ignored:failure of fibres, nonlinear elasticity and visco-elasticity of SMPs, delamination between SMPs and fibres. For the carbon fibres, the post-buckling produced large macro structural strain with small material strain, so carbon fibres considered as linear elasticity is reasonable. If carbon fibres break under large flexural deformation, the theoretical model in this paper cannot descript the phenomenon. For SMPs, which are considered as linear elasticity, it may introduce inaccuracy because of the existence of nonlinearity, viscoelasticity of SMPs. However, the deformation behaviour shows approximate linearity during the recovery process of SMPs around glass transition temperature (Lan et al., 2009; Leng et al., 2009b). Consequently, the mechanical behaviour of SMPs described as linear elasticity is considered to be reasonable in order to simplify the theoretical analysis process. For the SMPs composite, failure (delamination between SMPs and fibres, etc.) is also negative for the simplification.

In our future work, in order to describe the behaviour of thermal sensitivity, high visco-elasticity and large deformation of SMPs, we will construct free energy model integrating the linear elasticity, hyperelasticity and viscoelasticity. Based on this model, it is expected to achieve the constitutive relationship, and further study the buckling behaviour of SMPs.

7. Conclusions

This paper developed a buckling mechanical model of fibre-reinforced SMPC materials under the condition of large deflection deformation. The local post-buckling mechanics of unidirectional fibre-reinforced SMPC were investigated, and the problem of small strains and large displacements was considered. The cross section of a composite material under flexural deformation can be divided into three areas: the non-buckling stretching area, non-buckling compression area and buckling compression area. Three variables were identified: the critical buckling position, neutral plane position and fibre buckling half-wavelength. We determined the strain energy expression of the SMPC thermodynamic system. According to the least energy principle, we determined the analytical expressions of the key parameters in the flexural deformation process, including the critical buckling curvature k_c, critical buckling position z_{cb}, neutral plane position z_{ns}, buckling fibre wavelength λ, buckling fibre amplitude A and macroscopic strain of the composite material. The composite material began to perform fibre buckling when the curvature increased to the critical value k_c from infinitesimal curvature. When $k \geqslant k_c$, the neutral plane of the material z_{ns} moved towards the outboard tensile area, the critical buckling position z_{cb} moved towards the neutral plane z_{ns}, the half-wavelength λ decreased slowly, and the amplitude A_{max} and maximum strain ε_{max} of the inner compression plane increased at varying rates. Along with the increase of the shear modulus, the critical curvature k_c and the buckling amplitude A_c increased, while the fibre buckling critical half-wavelength λ_c decreased and the critical strain ε_c of the composite material increased. Greater composite stiffness led to smaller values of the buckling half-wavelength of the composite material. We conducted experiments to test the key parameters of the SMPC materials under flexural deformation. When the experimental values were compared to the theoretical values, our prediction is proved to be accurate. Based on the buckling deformation of the fibre, this paper uses the small material strain of the fibre to produce large geometrical displacement deformation of the composite material structure.

Acknowledgments

This work is supported by the National Natural Science Foundation of China (Grant Nos. 11102052, 11272106, 11225211, 51205076), China Postdoctoral Science Foundation (Garnt No. 2012M520032) and the Fundamental Research Funds for the Central Universities (Grant No. HIT.NSRIF.2013030).

References

Audoly, B., Boudaoud, A., 2008a. Buckling of a thin film bound to a compliant substrate – Part I: formulation, linear stability of cylindrical patterns, secondary bifurcations. Journal of the Mechanics and Physics of Solids 56, 2401–2421.

Audoly, B., Boudaoud, A., 2008b. Buckling of a thin film bound to a compliant substrate – Part II: a global scenario for the formation of herringbone pattern. Journal of the Mechanics and Physics of Solids 56, 2422–2443.

Audoly, B., Boudaoud, A., 2008c. Buckling of a thin film bound to a compliant substrate – Part III: herringbone solutions at large buckling parameter. Journal of the Mechanics and Physics of Solids 56, 2444–2458.

Barrett, R., Francis, W., Abrahamson, E., Lake, M.S. 2006. Qualification of elastic memory composite hinges for spaceflight applications. In: 47th AIAA/ASME/ASCE/AHS/ASC Structures, Structural Dynamics, and Materials Conference. 1–4 May 2006, Newport, Rhode Island, AIAA2006-20391∼10.

Cai, S., Breid, D., Crosby, A.J., Suo, Z., Hutchinson, J.W., 2011. Periodic patterns and energy states of buckled films on compliant substrates. Journal of the Mechanics and Physics of Solids 59, 1094–1114.

Cerda, E., Mahadevan, L., 2003. Geometry and physics of wrinkling. Physical Review Letters 90, 074302.

Chen, X., Hutchinson, J.W., 2004. Herringbone buckling patterns of compressed thin films on compliant substrates. Journal Applied Mechanics 71, 597–603.

Francis, W.H., Lake, M.S., Schultz, M.R., Campbell. D. 2007. Elastic memory composite microbuckling mechanics: closed-form model with empirical correlation. In: 48th AIAA/ASME/ASCE/AHS/ASC Structures, Structural Dynamics, and Materials Conference, 23–26 April 2007, Honolulu, Hawaii, AIAA2007-2164, pp. 1–16.

Huang, R., 2005. Kinetic wrinkling of an elastic lm on a viscoelastic substrate. Journal of the Mechanics and Physics of Solids 53, 63–89.

Huang, Z.Y., Hong, W., Suo, Z.G., 2004. Evolution of wrinkles in hard lms on soft substrates. Physical Review E 70, 030601.

Huang, Z.Y., Hong, W., Suo, Z.G., 2005. Nonlinear analyses of wrinkles in a film bonded to a compliant substrate. Journal of the Mechanics and Physics of Solids 53, 2101–2118.

Jiang, H.Q., Sun, Y.G., Rogers, J.A., Huang, Y.G., 2008. Post-buckling analysis for the precisely controlled buckling of thin film encapsulated by elastomeric substrates. International Journal of Solids and Structures 45, 2014–2023.

Lan, X., Wang, X.H., Liu, Y.J., Leng, J.S., 2009. Fiber reinforced shape-memory polymer composite, its application in a deployable hinge. Smart Materials and Structures 18, 024002.

Leng, J.S., Du, S.Y., 2010. Shape Memory Polymer and Multifunctional Composit. CRC Press.Taylor & Francis, pp. 293–314.

Leng, J.S., Lv, H.B., Liu, Y.J., Du, S.Y., 2008. Synergic effect of carbon black and short carbon fiber on shape memory polymer actuation by electricity. Journal of Applied Physics 104, 104917.

Leng, J.S., Lv, H.B., Liu, Y.J., Huang, W.M., Du, S.Y., 2009a. Shape memory polymers – a class of novel smart material. MRS Bulletin 34, 848–855.

Leng, J.S., Lan, X., Liu, Y.J., Du, S.Y., 2009b. Electroactive shape-memory polymer composite filled with nano-carbon powders. Smart Materials and Structures 18, 074003.

Leng, J.S., Wu, X.L., Liu, Y.J., 2009c. Effect of linear monomer on thermomechanical properties of epoxy shape-memory polymer. Smart Materials and Structures 18, 095031.

Leng, J.S., Liu, L.W., Liu, Y.J., Yu, K., Sun, S.H., 2009d. Electromechanical stability of dielectric elastomer. Applied Physics Letters 94, 211901.

Leng, J.S., Lan, X., Liu, Y.J., Du, S.Y., 2011. Shape-memory polymers and their composites: stimulus methods and applications. Progress in Materials Science 56, 1077–1135.

Li, B., Liu, L.W., Suo, Z.G., 2011. Extension limit, polarization saturation, and snap-through instability of dielectric elastomers. International Journal of Smart and Nano Materials 2 (2), 59–67.

Liu, Y.J., Liu, L.W., Zhang, Z., Shi, L., Leng, J.S., 2008. Comment on "Method to analyze electromechanical stability of dielectric elastomers". Applied Physics Letters 93, 106101.

Liu, Y.J., Liu, L.W., Sun, S.H., Shi, L., Leng, J.S., 2009. Comment "On electromechanical stability of dielectric elastomers". Applied Physics Letters 94, 096101.

Liu, Y.J., Liu, L.W., Zhang, Z., Jiao, Y., Sun, S.H., Leng, J.S., 2010. Analysis and manufacture of an energy harvester based on a Mooney–Rivlin-type dielectric elastomer. Europhysics Letters 90, 36004.

Liu, L.W., Liu, Y.J., Li, B., Yang, K., Li, T.F., Leng, J.S., 2011. Thermo-electro-mechanical stability of dielectric elastomers. Smart Materials and Structures 20, 075004.

Lu, H.B., Yu, K., Sun, S.H., Liu, Y.J., Leng, J.S., 2010. Mechanical and shape-memory behavior of shape-memory polymer composites with hybrid fillers. Polymer International 59, 766–771.

Lv, H.B., Liu, Y.J., Gou, J.H., Leng, J.S., Du, S.Y., 2010. Synergistic effect of carbon nanofiber and carbon nanopaper on shape memory polymer composite. Applied Physics Letters 96, 084102.

Ryu, S.Y., Xiao, J., Park, W., Son, K., Huang, Y., Paik, U., Rogers, J.A., 2009. Lateral buckling mechanics in silicon nanowires on elastomeric substrates. Nano Letters 9 (9), 3214–3219.

Suo, Z.G., 2010. Theory of dielectric elastomers. Acta Mechanica Solida Sinica 23 (6), 549–578.

Suo, Z.G., Zhao, X.H., Greene, W.H., 2008. A nonlinear field theory of deformable dielectrics. Journal of the Mechanics and Physics of Solids 56, 467.

Xiao, J., Ryu, S.Y., Huang, Y., Hwang, K.-C., Paik, U., Rogers, J.A., 2010. Mechanics of nanowire/nanotube in-surface buckling on elastomeric substrates. Nanotechnology 21, 085708.

Yu, K., Zhang, Z.C., Liu, Y.J., Leng, J.S., 2011. Carbon nanotube chains in a shape memory polymer/carbon black composite: to significantly reduce the electrical resistivity. Applied Physics Letters 98, 074102.